

# A Novel Tumor-Activated Prodrug Strategy Targeting Ferrous Iron Is Effective in Multiple Preclinical Cancer Models

Benjamin Spangler,<sup>†,‡</sup> Shaun D. Fontaine,<sup>‡,∇</sup> Yihui Shi,<sup>§</sup> Lidia Sambucetti,<sup>§</sup> Aras N. Mattis,<sup>||</sup> Byron Hann,<sup>⊥</sup> James A. Wells,<sup>‡,#</sup> and Adam R. Renslo<sup>\*,‡,⊕</sup>

<sup>†</sup>Graduate Program in Chemistry and Chemical Biology, University of California—San Francisco, San Francisco, California 94158, United States

<sup>‡</sup>Department of Pharmaceutical Chemistry, University of California—San Francisco, San Francisco, California 94158, United States

<sup>§</sup>SRI International, Menlo Park, California 94025-3493, United States

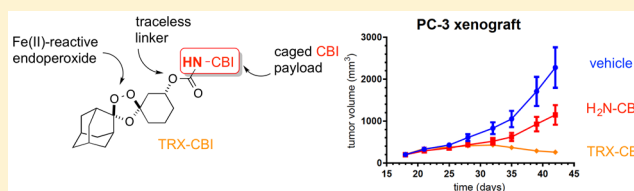
<sup>||</sup>Department of Pathology, University of California—San Francisco, San Francisco, California 94158, United States

<sup>⊥</sup>Preclinical Therapeutic Core, University of California—San Francisco, San Francisco, California 94158, United States

<sup>#</sup>Department of Cellular and Molecular Pharmacology, University of California—San Francisco, San Francisco, California 94158, United States

## Supporting Information

**ABSTRACT:** Here we describe a new approach for tumor targeting in which augmented concentrations of Fe(II) in cancer cells and/or the tumor microenvironment triggers drug release from an Fe(II)-reactive prodrug conjugate. The 1,2,4-trioxolane scaffold developed to enable this approach can in principle be applied to a broad range of cancer therapeutics and is illustrated here with Fe(II)-targeted forms of a microtubule toxin and a duocarmycin-class DNA-alkylating agent. We show that the intrinsic reactivity/toxicity of the duocarmycin analog is masked in the conjugated form and this greatly reduced toxicity in mice. This in turn permitted elevated dosing levels, leading to higher systemic exposure and a significantly improved response in tumor xenograft models. Overall our results suggest that Fe(II)-dependent drug delivery via trioxolane conjugates could have significant utility in expanding the therapeutic index of a range of clinical and preclinical stage cancer chemotherapeutics.



## INTRODUCTION

The recent development of molecularly targeted cancer therapeutics has been accompanied by renewed interest in technologies for the tumor/cell-selective delivery of potent but intrinsically nonselective cytotoxic agents. These technologies include antibody–drug conjugates (ADCs) that recognize cell-surface antigens and tumor-activated prodrugs (TAPs) that exploit nutrient transporters<sup>1–3</sup> or differences in hypoxia associated with the tumor microenvironment.<sup>4,5</sup> Accumulating evidence suggests that an increase in reactive, “labile” intracellular iron is another metabolic signature of cancer, as recently reviewed.<sup>6</sup> Tumor targeting strategies designed to exploit changes in iron homeostasis remain largely unexplored however, despite clinical precedent for iron-dependent pharmacology in antimalarial therapy with artemisinins.<sup>7,8</sup>

Redox cycling of iron in enzyme cofactors is essential for cellular processes ranging from de novo nucleotide synthesis to the maintenance of genomic stability, cell cycle regulation, and mitochondrial respiration.<sup>6</sup> However, when unbound and unregulated, redox active iron promotes the disproportionation of hydrogen peroxide (Fenton reaction) to produce hydroxyl and hydroperoxyl radicals, reactive oxygen species (ROS) that confer cellular damage and can lead to apoptosis or

ferroptosis.<sup>9–11</sup> Iron homeostasis is therefore highly regulated to ensure sufficient labile iron is available to support essential enzyme function while limiting exposure to unbound, redox active iron species.<sup>12–14</sup>

Rapidly proliferating cells have increased requirements for DNA synthesis, repair, and mitochondrial respiration and therefore have increased demands for iron cofactor biosynthesis. Accordingly, iron acquisition and export pathways are altered in many cancers so as to increase the labile iron pool.<sup>6,15–18</sup> Furthermore, iron has been shown to contribute to tumor initiation and growth<sup>15,19</sup> and epidemiological evidence has established links between tumor iron metabolism and clinical outcomes in breast cancer patients.<sup>17,20</sup> Given that labile Fe(II) promotes Fenton chemistry, we sought to develop a tumor-targeting strategy in which Fenton reaction of a peroxidic prodrug was coupled to release of drug payloads. Recognizing that antimalarial agents such as arterolane<sup>21–24</sup> exhibit finely tuned iron(II) reactivity,<sup>25–28</sup> we subsequently developed<sup>29,30</sup> an arterolane-inspired small molecule platform (denoted TRX herein) for Fe(II)-dependent drug delivery.

Received: October 7, 2016

Published: November 21, 2016

These TRX-drug conjugates function via initial Fe(II)-promoted fragmentation of a 1,2,4-trioxolane ring to afford a cyclohexanone intermediate, followed by spontaneous  $\beta$ -elimination and decarboxylation to release the drug payload (Figure 1 and Supporting Information Figure S1). In previous

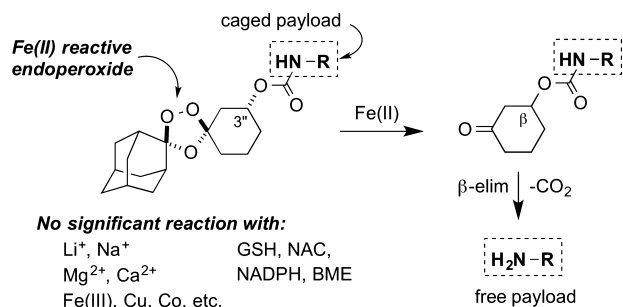


**Figure 1.** Mechanism of iron(II)-dependent payload release from 1,2,4-trioxolane conjugates. Iron(II)-promoted Fenton-type reduction of the trioxolane ring affords the cyclohexanone species shown which then undergoes spontaneous  $\beta$ -elimination and decarboxylation to release free payload. This process occurs with high efficiency and ferrous-iron selectivity in mammalian cancer cell lines, as described recently.<sup>34</sup>

studies, we demonstrated the utility of the TRX scaffold by efficiently and selectively delivering antimalarial payloads to ferrous iron/heme rich compartments of the malaria parasite, both in vitro<sup>30,31</sup> and in vivo.<sup>32,33</sup>

While the iron-dependent pharmacology of 1,2,4-trioxanes and 1,2,4-trioxolanes in malaria is widely accepted,<sup>25–28</sup> extending this concept to TAPs for oncology applications required a means to assess whether sufficient labile iron is present in cancer cells to efficiently and selectively activate TRX-based conjugates. To address this question, we synthesized a TRX conjugate of the aminonucleoside antibiotic puromycin (i.e., TRX-PURO) as a probe of intracellular labile iron (Figure 1 where R–NH<sub>2</sub> = puromycin). We found that puromycin release from TRX-PURO in cells was dependent on ferrous iron as expected and was not affected by the addition of other biologically relevant metal ions and reducing agents.<sup>34</sup> These initial studies with TRX-PURO also confirmed that labile iron pools are generally augmented in cancer cells when compared to nontumorigenic cells.<sup>34</sup> Our findings thus suggested that the TRX scaffold might indeed be applied to produce a novel class of TAPs for cancer chemotherapy.

Here we describe prototypical TRX-drug conjugates designed to confer tumor-selective delivery of a microtubule toxin (a combretastatin analog) or DNA-alkylating agent (a duocarmycin analog) in an Fe(II)-dependent fashion. We show that the intrinsic cytotoxicity of these agents can be ablated in TAP forms and then restored following activation in cancer cells. We show that cancer cell lines of diverse origins are generally susceptible to TRX-based TAPs but that a nontumorigenic cell line (MCF10A) is highly resistant. We further show that the resistant MCF10A cell line can be measurably sensitized to the TAP when transformed with the oncogene cMyc and that this likely derives from oncogenic changes to iron metabolism. Finally, we show that the TAP of a duocarmycin analog is tolerated in mice at doses up to 50-fold higher than the parent cytotoxin and this, combined with targeted toxin release within tumor, translates to superior efficacy in PC-3 and MDA-MB-231 xenograft models. These

studies provide the first evidence that reactive iron in tumor cells and/or the tumor microenvironment can be exploited to afford improved selectivity in the delivery of cancer chemotherapeutics.

## RESULTS

**Conjugate Design, Synthesis, and Validation in Cell Culture.** To explore ferrous iron-dependent drug delivery in cancer cells we synthesized a known small molecule microtubule toxin (1)<sup>35</sup> and its trioxolane conjugate 2 (Figure 2a and Supporting Information Figure S2). A nonperoxidic dioxolane conjugate (3) was also prepared to confirm that the cytotoxicity of 1 is ablated in conjugated forms and that intracellular release of active 1 from 2 is peroxide-dependent (Figure 2a and Figure S2). Finally, trioxolane analog 4<sup>29</sup> lacking the microtubule toxin moiety (Figure 2a). The cytotoxicity of the trioxolane-conjugate 2 and control compounds 1, 3, and 4 was then assessed across a small panel of cell lines. The results were unequivocal. In MDA-MB-231 cells, trioxolane-conjugate 2 displayed activity in the low nM range (EC<sub>50</sub> = 21 nM), 3 orders of magnitude more potent than either of the negative controls (3 or 4) and nearly as potent as the free toxin (1) applied directly (EC<sub>50</sub> = 11 nM) (Figure 2b). These results confirm that release of 1 from 2 in these cells is both efficient and peroxide-dependent. Moreover, the lack of measurable toxicity exhibited by 3 demonstrates that the intrinsic cytotoxicity of 1 is effectively blocked in TAP form.

Normalizing the activity of conjugate 2 to that of its cytotoxic payload (1) provided a convenient metric (“EC<sub>50</sub> ratio”) to compare efficiency of payload release from 2 across different cell lines. In MDA-MB-231 cells, this ratio was found to be 0.54 (EC<sub>50</sub> = 11 nM and 21 nM for 1 and 2, respectively). Among the other cell lines examined, U2OS and RKO cells were nearly as susceptible to 2 as MDA-MB-231 cells (EC<sub>50</sub> ratio of 0.46) while PC-3 and HeLa cells were somewhat less sensitive (EC<sub>50</sub> ratio of 0.30–0.32), though 2 was still effective in these cells at therapeutically relevant, low-nM concentrations (Figure 2d and Supporting Information Table S1). Consistent with our previous finding that nontumorigenic cells possess a smaller reactive iron pool,<sup>34</sup> MCF10A cells were highly resistant to the trioxolane-conjugate 2 with an EC<sub>50</sub> ratio of just 0.04 (Figure 2c,d).

Encouraged by these initial findings, we further explored the cytotoxicity of 1 and 2 across a larger panel of cancer cell lines from diverse origins using a CellTiter-Glo assay to assess cell viability (Figure 2e). We found EC<sub>50</sub> ratios varied by about 9-fold across the different cell lines, from 0.89 for the most susceptible cells (PC-3) cells to 0.11 for the least susceptible cells (EKVX). Despite the range of responses, TAP 2 produced EC<sub>50</sub> values in the nM range for even the least responsive cell lines (e.g., EKVX EC<sub>50</sub> = 43 nM, Supporting Information Table S2). As expected, the EC<sub>50</sub> values for trioxolane control 4 across this panel were in the  $\mu$ M regime and typically  $\geq 2$  log units less potent than 2 (Supporting Information Table S2). This confirms that the cytotoxicity of TAP 2 derives from release of 1 and not significantly from the trioxolane moiety itself.

**Oncogenic Transformation and Susceptibility to Trioxolane Conjugates.** Having found that nontumorigenic MCF10A cells were highly resistant to TRX-conjugates, we explored whether oncogenic transformation of these cells would increase their reactive iron pools and thus sensitize them to trioxolane conjugates. Bandyopadhyay and co-workers

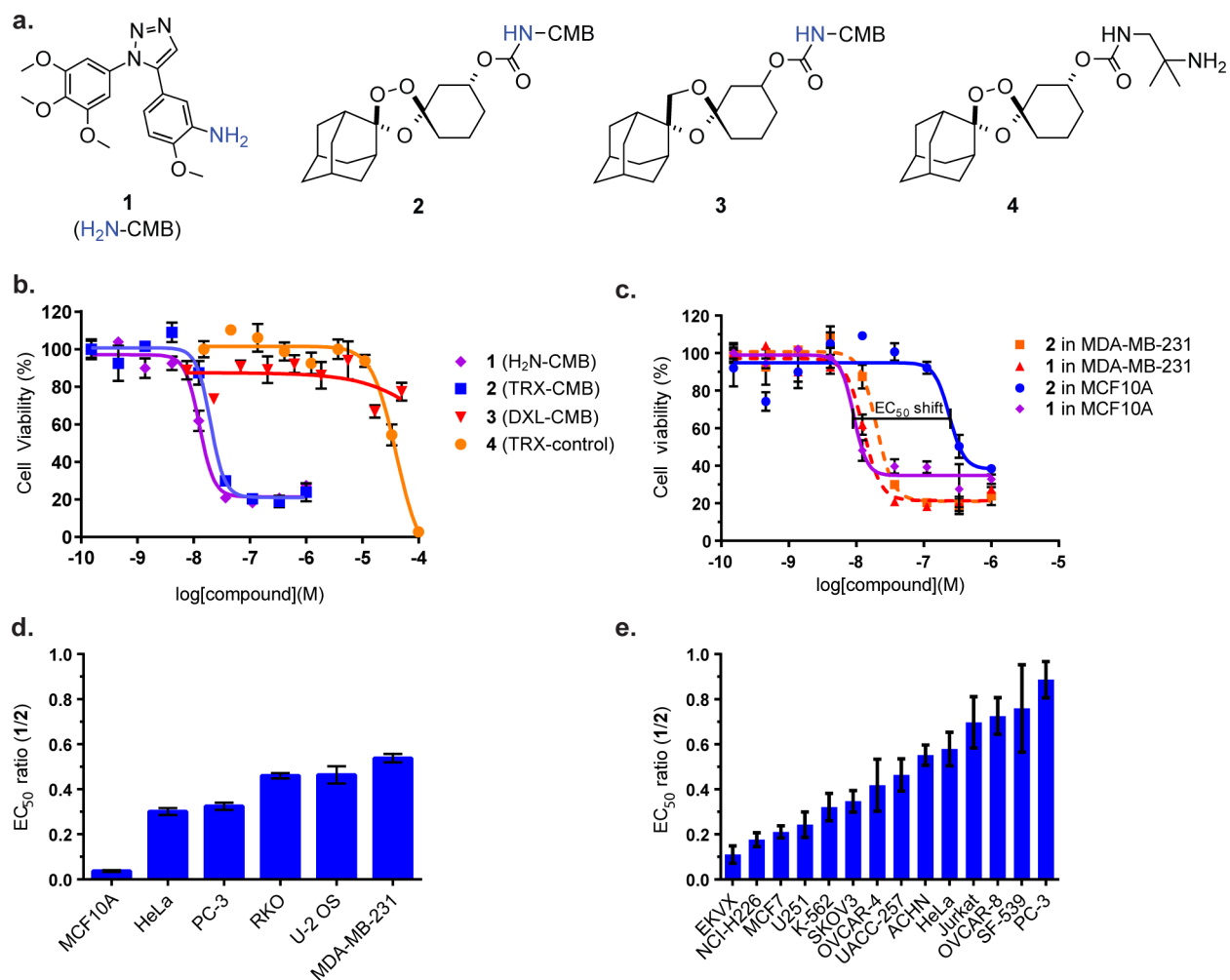


**Figure 2.** Exploiting augmented ferrous iron pools for selective drug delivery. (a) Chemical structure of microtubule inhibitor **1** and corresponding conjugates and controls **2**–**4**. (b) Cytotoxicity of compounds **1**–**4** in MDA-MB-231 cells after 24 h of exposure as determined by cell counting ( $n = 3$ ; error bar, mean  $\pm$  SEM). (c) Cytotoxicity of **1** and its trioxolane-conjugate **2** after 24 h of exposure in MDA-MB-231 and MCF10A cells as determined by cell counting ( $n = 3$ ; error bar, mean  $\pm$  SEM). The shift in EC<sub>50</sub> value for **1** and its trioxolane conjugate **2** is illustrated. Dividing the EC<sub>50</sub> value for **1** by that for **2** in a given cell line produces an “EC<sub>50</sub> ratio” that is used to compare the efficiency of drug release across cell lines. This ratio is 0.54 for sensitive MDA-MB-231 cells (2-fold EC<sub>50</sub> shift) and 0.04 for relatively resistant, nontumorigenic MCF10A cells (25-fold EC<sub>50</sub> shift). (d) EC<sub>50</sub> ratios calculated as described in (c) for a small panel of cell lines. Error bars represent SEM from three individual experiments each conducted in biological triplicates. (e) EC<sub>50</sub> ratios for an expanded panel of mammalian cell lines. The EC<sub>50</sub> values for **1** and **2** were determined after a 72 h incubation using the CellTiter-Glo cell viability assay. Error bars represent SEM ( $n = 3$ ).

recently reported the generation of a panel of cell lines expressing single oncogenes in MCF10A cells.<sup>36</sup> Using these well-characterized cell lines, we examined the effects of the oncogenes Ras and Myc, whose effects on iron metabolism have been studied previously.<sup>6,16,18,37,38</sup> First, we used qRT-PCR to evaluate the transcriptional profile of a panel of iron regulatory proteins in the MCF10A cells constitutively expressing HRas. In previous work in different cell types, oncogenic HRas has been variously reported to decrease ferritin mRNA levels and increase labile iron<sup>38</sup> or to have no effect on ferritin levels or labile iron.<sup>16</sup> In the MCF10A cells expressing HRas we observed no significant transcriptional changes to ferritin, transferrin receptor, or any other of the iron regulatory transcripts probed (Figure 3 and Supporting Information Figure S3). It was therefore unsurprising that the HRas-expressing MCF10A cells were no more susceptible to **2** than MCF10A cells transformed with the empty vector (Figure 3b). In contrast, MCF10A cells transformed with cMyc showed substantial down regulation of the iron exporter ferroportin and

up regulation of the ferrireductase STEAP3 (Figure 3a). Interestingly, we did not observe an effect of cMyc on ferritin heavy chain mRNA, as has been reported previously.<sup>18</sup> Nevertheless, the changes observed predict for increased labile iron in the cMyc-transformed MCF10A cells, and indeed, these cells were found to be more sensitive to trioxolane-conjugate **2** than cells transformed with the empty vector, as evidenced by a significant 3.2-fold shift in the EC<sub>50</sub> ratio (Figure 3b). These results indicate that oncogene induced changes to the reactive iron pool can sensitize cells to the delivery of potent cytotoxins from TRX-based TAPs in an otherwise isogenic background.

#### In Vivo PK/PD Studies of a Duocarmycin Conjugate.

The highly cytotoxic cyclopropylbenzindoline (CBI) class of natural products like CC-1065 and duocarmycin SA function by alkylating adenine bases in duplex DNA.<sup>39–42</sup> Synthetic “seco”-CBI analogs are latent cytotoxins that can undergo spontaneous Winstein-type spirocyclization to form the active cyclopropylbenzindoline (CBI) species (i.e., *seco*-**5**  $\rightarrow$  **5**, Figure 4a and Supporting Information Figure S4). This activation step can be

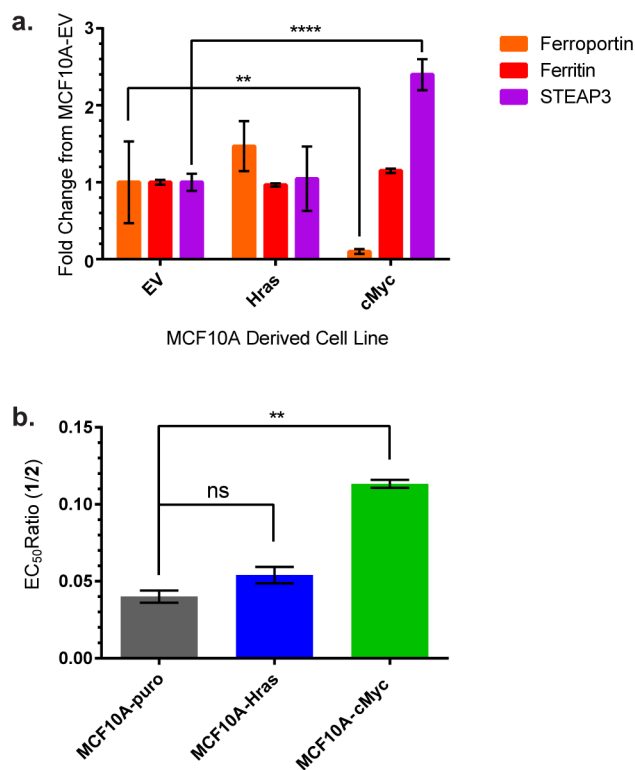


**Figure 3.** Profiling the effects of oncogenic transformation on the ferrous iron pool of MCF10A cells. (a) Relative mRNA levels for ferroportin, ferritin, and the ferrireductase STEAP3 in MCF10A cells stably transfected with empty vector (control) or with vectors expressing the oncogenes Myc or Hras ( $n = 3$ ; error bar, mean  $\pm$  SEM; (\*\*\*)  $P \leq 0.01$ , (\*\*\*\*)  $P \leq 0.0001$ , two-way ANOVA with Dunnett's multiple comparisons test). (b) EC<sub>50</sub> ratio (1/2) for MCF10A cells stably transfected with HRas or cMyc oncogenes or the empty vector (control) as assessed by cell counting after 24 h of compound exposure. Error bars represent SEM from three independent experiments each conducted in biological triplicates ((\*\*)  $P \leq 0.01$ , one-way ANOVA with Dunnett's multiple comparisons test).

prevented by acylation or carbamoylation of the aniline or phenolic function, and the ability to “cage” *seco*-CBI derivatives in this way has made these compounds popular as cytotoxic effectors in antibody–drug conjugates<sup>2,42</sup> and tumor-activated prodrugs.<sup>3,41</sup> We synthesized a known *seco*-CBI analog<sup>40</sup> and further converted the material into the desired TAP 6 and the 1,3-dioxolane-CBI conjugate 7 (DXL-CBI), a nonperoxidic control (Figure 4a).

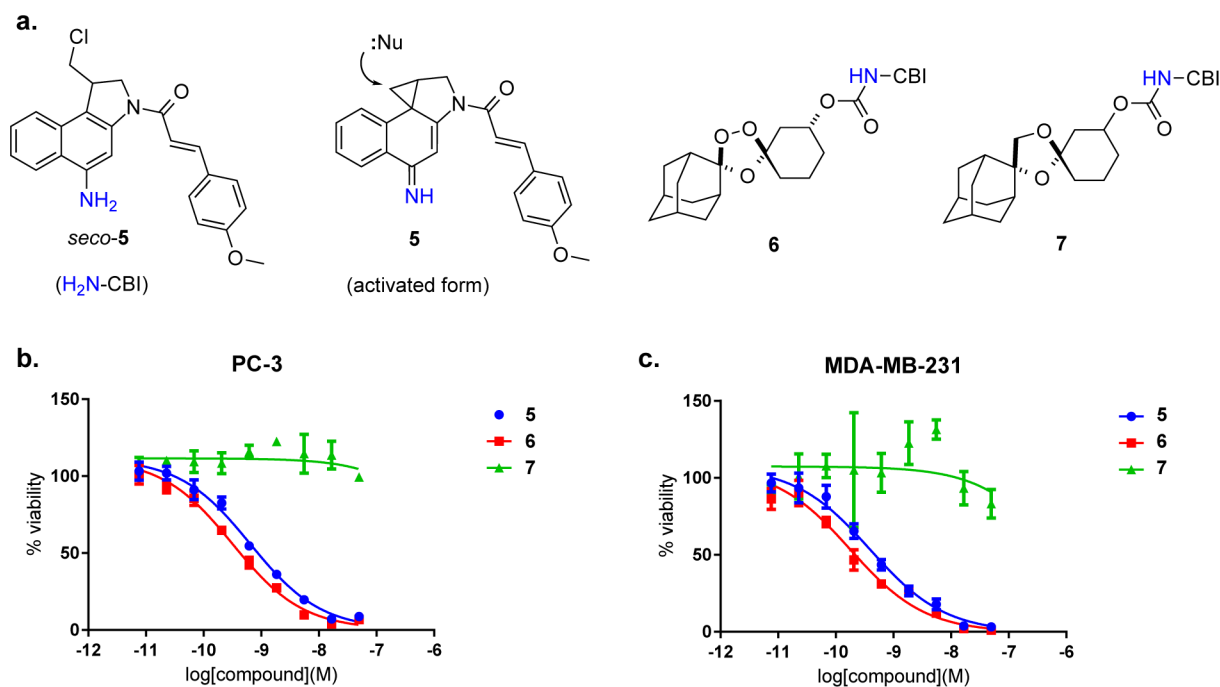
We evaluated the cytotoxicity of *seco*-5, TAP 6, and control 7 following 72 h of exposure in MDA-MB-231 and PC-3 cells (Figure 4b,c). As expected, *seco*-5 and its TAP 6 exhibited potent cytotoxic effects in cells, while the dioxolane conjugate 7 was nontoxic at all concentrations examined. The inactivity of 7 confirms that conjugation of *seco*-5 via its aniline function effectively blocks formation of the activated (and toxic) CBI electrophile. The potent effects of 6 in cells are thus due to peroxide-dependent release of free *seco*-5 as desired. We further found that conversion of *seco*-5 to the TAP 6 dramatically improves its chemical stability in the extracellular environment. Thus, while free *seco*-5 degraded over several hours upon thawing from a DMSO stock solution, TRX conjugate 6 (and DXL conjugate 7) were chemically stable for more than a year at room temperature in DMSO (Supporting Information

Figure S5). Stability toward premature hydrolysis likely explains why TAP 6 was measurably more potent than *seco*-5 itself in both cell lines examined (Figure 4b,c). Control experiments confirmed that 6 is stable for more than a week in cell culture media at 37 °C, indicating that its cellular toxicity in the 72 h assays (Figure 4b,c) results from intracellular release of *seco*-5 as desired.

The cell culture studies of 5–7 above revealed the effective ablation of 5-mediated toxicity by chemical conjugation at an aniline function (Figure 4a–c). We next asked whether this caging effect would translate to reduced in vivo toxicity for TAP 6 as compared to 5. To determine a maximally tolerated dose (MTD), nontumor bearing female NSG mice were administered three ip doses of either *seco*-5 or 6 at 4-day intervals (Q4d). These studies revealed that *seco*-5 is highly toxic to mice (MTD  $\approx$  0.3 mg/kg), consistent with previous observations for related duocarmycin analogs.<sup>41</sup> By contrast, TAP 6 could be administered at significantly higher doses, with an MTD of 7.5 mg/kg, using the same three dose Q4d regimen. A subsequent MTD study of 6 with Q7d dosing returned a somewhat higher MTD of  $\sim$ 10 mg/kg.

Previous work with duocarmycin analogs related to 5 has shown dose-limiting hepatotoxicity in mice<sup>43</sup> and insufficient therapeutic index leading to failures in human clinical trials.<sup>44</sup> We were therefore interested in exploring the toxic effects of 5 in mice and whether administration in the TRX-conjugated form 6 could protect from these toxicities. In fact, mice treated with 0.3 mg/kg *seco*-5 showed substantially ( $\sim$ 10-fold) higher concentrations of liver transaminase enzymes (ALT and AST) than did mice treated with 7.5 mg/kg of 6 (Figure 5c). Since hepatotoxicity of duocarmycin analogs has previously been observed to occur with a delayed onset, mice receiving escalating doses of 5 or 6 were observed for 50 days postdosing, then sacrificed and their livers collected and assessed for altered morphology and signs of toxicity. Even at well-tolerated doses of 5, mice grossly showed darkened and roughened capsular and parenchymal changes indicative of hepatotoxicity in addition to enlarged intestines and seroanguinous ascites near the site of administration. The liver pathology showed increased hepatic lobular lymphohistiocytic infiltrates, reactive cellular changes, and minimal periportal fibrosis. In contrast, the livers of mice treated with 7.5 mg/kg of 6 appeared normal, and the dose limiting toxicity appeared instead to be localized toxicity at the site of administration as evidenced by enlarged intestines. The pathology in these was free of significant inflammation or fibrosis (Figure 5d).

To compare the pharmacokinetic properties of *seco*-5 and its TRX conjugate 6, healthy NSG mice were administered a single ip dose of *seco*-5 (0.3 mg/kg) or conjugate 6 (7.5 mg/kg), representing the respective MTD values. Analysis of blood samples showed *seco*-5 to have a reasonably long half-life ( $t_{1/2} = 3.8$  h), moderate clearance ( $CL/F = 20$  mL min<sup>-1</sup> kg<sup>-1</sup>) and a high volume of distribution ( $V_z/F = 6.7$  L/kg) (Figure 5a,b, Supporting Information Table S3). Conjugate 6 exhibited a significantly longer half-life ( $t_{1/2} = 20.4$  h), moderate-high clearance ( $CL/F = 31.3$  mL min<sup>-1</sup> kg<sup>-1</sup>) and a very high volume of distribution ( $V_z/F = 55$  L/kg). In animals receiving 6, total exposure to 6 (AUC = 5050 h·ng/mL) exceeded that of released *seco*-5 by approximately 8-fold, indicating a small degree of drug release in normal tissues of healthy mice. Maximum plasma concentrations of free *seco*-5 in mice receiving 7.5 mg/kg of 6 were still lower than those in mice treated with 0.3 mg/kg of *seco*-5 directly ( $C_{max} = 48$  ng/mL vs



**Figure 4.** Structures and in vitro activity of trioxolane–duocarmycin conjugates. (a) Structure of duocarmycin type DNA-alkylator *seco*-5 (latent form), the corresponding activated form 5 that reacts with nucleophilic bases of DNA (:Nu), trioxolane–duocarmycin conjugate 6, and negative control dioxolane–conjugate 7. (b) Cytotoxicity of compounds 5 and 6 in PC-3 cells after 72 h of exposure as determined by cell counting ( $n = 3$ ; error bar, mean  $\pm$  SEM). (c) Cytotoxicity of compounds 5 and 6 in MDA-MB-231 cells after 72 h of exposure as determined by cell counting ( $n = 3$ ; error bar, mean  $\pm$  SEM).

108 ng/mL). Most importantly, the total systemic exposure of 6 was  $\sim$ 20-fold greater than for *seco*-5 when both agents were administered at their respective MTD ( $AUC_{0-24h} = 5050$  and 246 h·ng/mL, respectively). The higher in vivo exposure achievable with TAP 6 was thus expected to result in superior efficacy in tumor bearing mice, where 6 would be converted to the active agent (5) selectively in the tumor.

To see whether the higher in vivo exposure levels achievable with conjugate 6 translated to improved in vivo efficacy, we treated PC-3 and MDA-MB-231 xenograft-bearing mice with 6 or *seco*-5 and compared body weights and rates of tumor growth under different dosing regimens (Figure 6). In MDA-MB-231 xenograft mice, three 0.3 mg/kg doses of *seco*-5 given Q4d produced only a minor reduction in the rate of tumor growth (Figure 6a). Significantly, the mice in this group showed substantial weight loss over the course of the study, presumably reflecting compound-related toxicity (Figure 6b). Comparatively, mice treated under the same regimen with 2.5 mg/kg of 6 exhibited a similar reduction in tumor growth rate but unlike 5-treated mice had negligible weight loss, suggesting reduced toxicity under a comparably efficacious regimen (Figure 6a). Using the same regimen but increasing the dose of 6 to its MTD of 7.5 mg/kg produced a substantially improved effect on tumor growth and with much less severe weight loss than was observed with a 25-fold lower dose of *seco*-5 (Figure 6a,b). These findings were replicated in a follow-up study that also included the evaluation of dioxolane conjugate 7 (Supporting Information Figure S6). As expected, compound 7 at 10 mg/kg had no effect on tumor growth or mouse weight, indicating that the beneficial in vivo effects of 6 result from peroxide-dependent activation and release of 5 in tumor.

The results described above for MDA-MB-231 xenograft mice were qualitatively replicated in PC-3 xenograft bearing

mice. Thus, administration of 6 at 7.5 mg/kg (3 $\times$ , Q4d, ip) produced comparable if not superior effects on tumor growth rate without the weight loss observed in mice receiving *seco*-5 at 0.3 mg/kg (Figure 6c,d). Since the MTD and pathology studies had suggested that the dose-limiting toxicity of TAP 6 was localized GI toxicity near the site of administration, we considered that an altered dosing regimen might mitigate this toxicity and enable a higher dose. Indeed, by increasing the dose of 6 to 15 mg/kg but extending the dosing interval from Q4d to Q7d (once weekly), we observed robust tumor regression (Figure 6c, orange line), albeit with weight loss that was similar to the animals receiving the 0.3 mg/kg Q4d regimen of 5. The tumor regression produced with 15 mg/kg Q7d dosing of 6 was found to be quite durable, with no evidence of further tumor growth observed for the remainder of the study, several weeks after the third and final dose.

## DISCUSSION

The search for more effective and better tolerated cancer therapies has yielded the first molecularly targeted agents<sup>45,46</sup> (e.g., kinase inhibitors, PARP inhibitors) and new technologies to more selectively deliver potent cytotoxins to tumors (e.g., antibody–drug conjugates). Herein we have described a new class of tumor activated prodrugs engineered to release a drug payload upon encountering reactive iron(II) in the tumor microenvironment. The trioxolane-based scaffold employed in these studies is the same one we used previously to study intracellular labile ferrous iron in cells, revealing larger iron(II) pools in cancer-derived cell lines compared to nontumorigenic lines.<sup>34</sup> Here we exploited this knowledge and the tools we developed to deliver cytotoxic payloads to diverse cancer cell lines and to target tumors in two different mouse xenograft models.

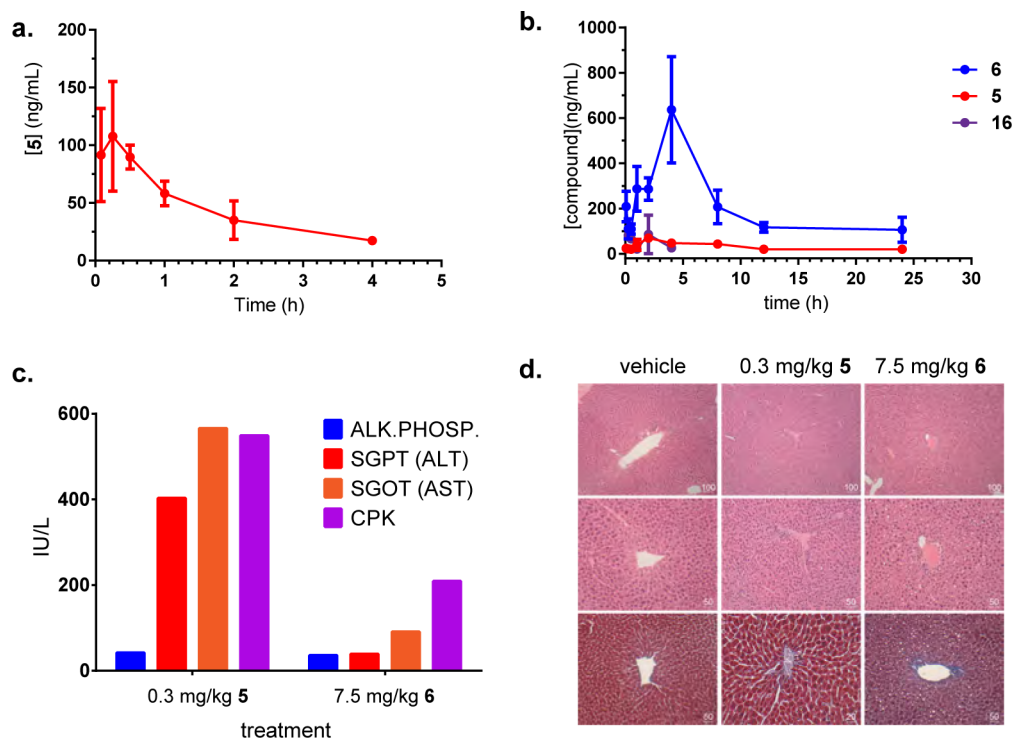


**Figure 5.** Pharmacokinetic profile and in vivo tolerability of **5** and its trioxolane conjugate **6**. (a) Plasma concentrations of **5** in female NSG mice following a single 0.3 mg/kg ip dose. Three mice were sampled at each time point. (b) Plasma concentrations of **6**, released **5**, and the retro-Michael intermediate **16** in female NSG mice following a single 7.5 mg/kg ip dose of **6**. An authentic sample of **16** was synthesized as described in the Supporting Information. The study design and numbers of mice per group were the same as in (a). (c) Measured levels of alkaline phosphatase (Alk. Phosp.), serum alanine aminotransferases (ALT), aspartate aminotransferase (AST), and creatine phosphokinase (CPK) in blood samples from mice treated with either **5** (0.3 mg/kg) or trioxolane-conjugate **6** (7.5 mg/kg). (d) Microscopic histology stains of representative mouse liver samples show only mildly increased reactive changes in the group receiving 0.3 mg/kg **5**, including minimally increased lobular lymphohistiocytic infiltrates. In mice receiving the higher 7.5 mg/kg dose of **6** (right column), only mild simple steatosis was detected. Top two rows of images show representative H&E sections of centrilobular or periportal areas. Bottom row of images show representative trichrome stains for evaluation of relative fibrosis, which shows no significant fibrosis; scale bars are in  $\mu\text{m}$  as indicated.

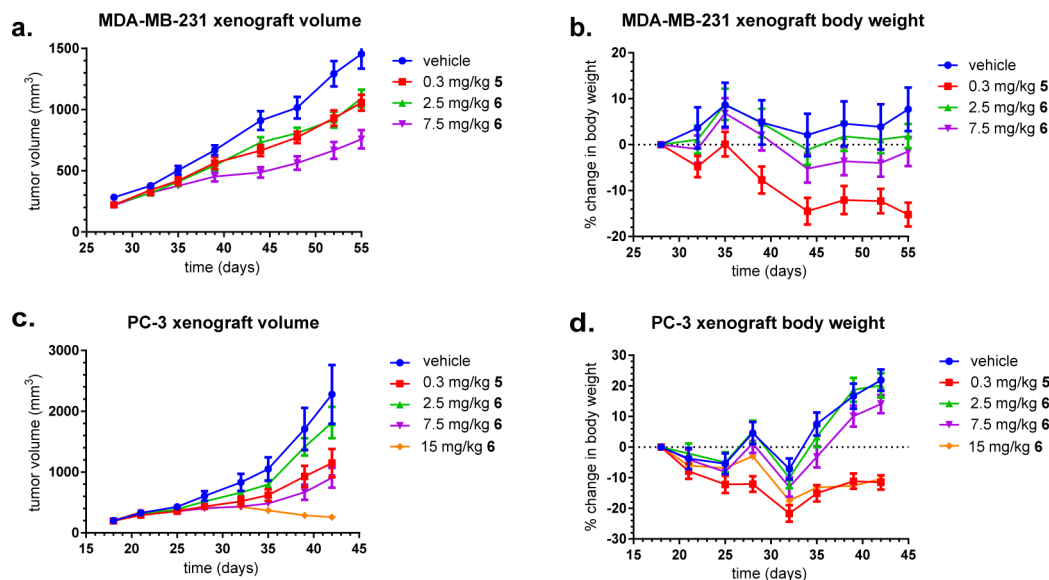


**Figure 6.** Efficacy of **5** and **6** in mouse xenograft models. (a) Changes in tumor volume over time as determined by calipers in MDA-MB-231 xenograft bearing female SCID-beige mice treated with the indicated doses of **5** or **6** via ip administration on a Q4d dosing schedule (3 total doses) as compared to mice treated with vehicle. Error bars represent SEM from dosing cohorts of 8 mice per condition. (b) Changes in mouse weight over time for the mice in (a). (c) Changes in tumor volume over time as determined by calipers in PC-3 xenograft bearing female nude mice (NCR nu/nu, Taconic) treated with the indicated doses of **5** or **6** via ip administration on a Q4d dosing schedule (3 total doses) as compared to mice treated with vehicle. Mice treated with the highest dose of **6** (15 mg/kg, orange line) received three ip doses on a Q7d schedule. Error bars represent SEM from dosing cohorts of 8 mice per condition. (d) Changes in mouse weight over time for the mice in (c).

The trioxolane TAP scaffold used here was engineered to confer “traceless” release of drug payloads, thereby enabling a broad scope of potential applications encompassing molecularly targeted and generally cytotoxic agents possessing suitable amine or alcohol functionality for conjugation. When this strategy is employed, the site of drug conjugation is selected so that the intrinsic activity/toxicity of tethered drug is ablated, thereby preventing or minimizing exposure of active drug in nontargeted tissues. To exemplify this approach, we prepared amine-linked TAP conjugates **2** and **6** from the microtubule inhibitor **1** and duocarmycin analog *seco-5*, respectively. We confirmed that the activity/toxicity of these agents was ablated in the TAP form by preparing dioxolane-drug conjugates **3** and **7**, which proved inactive at the highest concentrations tested (Figure 2b and Figure 4b,c). The lack of measurable activity for **3** and **7** thus confirms that drug release from **2** and **6** is peroxide dependent. Consistent with the expected mechanism of iron(II)-dependent drug release, the relative sensitivity of cells to **2** (Figure 2d) largely mirrored the response of the TRX-PURO probe to intracellular labile iron in the same cell lines.<sup>34</sup>

We found that sensitivity to TRX-CMB conjugate **2** varied by about 9-fold across a panel of cancer cell lines from diverse origins (Figure 2e). Further interrogation of these data may provide insight into the specific alterations of iron metabolism that predict for increased tumor susceptibility toward TRX-drug conjugates. In our preliminary study of oncogenic changes and related effects on iron metabolism, we observed that Myc-driven changes in MCF10A cells produced increased sensitivity to trioxolane conjugate **2**. Consistent with these observations, several of the most 2-susceptible cell lines examined here, such as RKO and MDA-MB-231, are known to overexpress Myc.<sup>36,47</sup> Thus, iron(II)-dependent drug delivery could find utility in targeting Myc-driven tumors indirectly via the alteration of iron metabolism induced by this prevalent oncogene. These findings are particularly relevant given how intractable Myc driven tumors have been toward other targeted therapies.<sup>48</sup>

To examine the utility of trioxolane-mediated drug delivery in vivo, we prepared trioxolane TAP **6** in which a potent duocarmycin-class cytotoxin (*seco-5*) is stabilized chemically and inactivated biologically (while in prodrug form). Significantly, conjugate **6** was tolerated in mice at doses up to 50-fold higher than *seco-5* and produced superior efficacy in two different xenograft models when administered at or near its MTD. A pharmacokinetic study in healthy mice revealed that administration of *seco-5* in the form **6** not only limited exposure to free drug (to ~15% of the total dose) but also significantly improved distribution to tissues and the total duration of drug exposure. These properties of **6** enabled safe administration at a relatively high dose of 15 mg/kg once weekly, and this dosing regimen produced a particularly robust and durable tumor regression in a PC-3 xenograft model. Overall, our studies indicate that trioxolane-based TAPs release their drug payload in proportion to the concentration of labile iron(II) encountered in different cell/tissue types. While intracellular iron(II) pools are likely implicated in TAP activation, it is possible that other aspects of tumor biology in vivo (e.g., hypoxia, macrophage infiltration, tumor necrosis) contribute to the presence of excess reactive iron(II) in the tumor microenvironment.

In conclusion, trioxolane-mediated iron(II)-dependent drug delivery is a new approach for cell/tissue selective drug targeting that leverages elevated reactive iron(II) concen-

trations in tumor cells and in the tumor microenvironment. Here we described two prototypical trioxolane-drug conjugates bearing cytotoxins with distinct mechanisms of cellular toxicity. We confirmed that the intrinsic toxicity of these agents could be ablated in conjugated forms and yet fully realized following cell- or tumor-selective release at their intended site of action. These results should encourage further study of this concept to identify drugs and tumor types that best leverage this new drug delivery approach.

## EXPERIMENTAL SECTION

The known cytotoxic agents **1**<sup>35</sup> and *seco-5*<sup>40</sup> were prepared as previously described. These compounds were coupled to known trioxolane<sup>29</sup> and dioxolane<sup>30</sup> intermediates via activated nitrophenyl carbonate or isocyanate intermediates as we have described previously<sup>29–31</sup> and as further detailed in the Supporting Information.

All compounds tested in cells or animals were judged to be of >95% purity as determined using a Waters Micromass ZQTM, equipped with Waters 2795 separation module, Waters 2996 photodiode array detector (254 nm), and Waters 2424 ELS detector. Separations were carried out with an XTerra MS C18, 5  $\mu$ m, 4.6 mm  $\times$  50 mm column, at ambient temperature (unregulated) using a mobile phase of water–methanol containing a constant 0.10% formic acid. Representative LC chromatograms are provided in the Supporting Information.

Mammalian cell lines were maintained in an atmosphere of 5% CO<sub>2</sub> in RPMI 1640 media purchased from HyClone supplemented with 10% FBS (Gibco), Pen/Strep (1 $\times$  final concentration, Gemini Bio-Products), and nonessential amino acids (UCSF Cell Culture Facility). Unless otherwise noted, cell lines were obtained from ATCC and verified by STR profiling. Graphing and analysis of data were done using GraphPad Prism 6 software and Microsoft Excel 2010. Figures were prepared with Adobe Design Standard CS6 software.

**Statistics.** Error bars in all figures represent SEM unless otherwise indicated. When three or more mean values were compared, one- or two-way ANOVA tests were applied as required with Dunnett’s multiple comparisons tests used to determine significance. Statistical significance is indicated as follows: \* =  $P \leq 0.05$ , \*\* =  $P \leq 0.01$ , \*\*\* =  $P \leq 0.001$ , \*\*\*\* =  $P \leq 0.0001$ .

**Toxicity by Nuclei Counting.** Cells were plated in 96-well Greiner black  $\mu$ Clear tissue culture plates at 3000–6000 cells per well in RPMI 1640 cell culture media (or the appropriate growth medium as specified) and incubated at 37  $^{\circ}$ C in 5% CO<sub>2</sub> incubators for at least 16 h prior to exposure to compounds. Cells were then treated in triplicate with escalating concentrations of compounds performed in medium containing 0.1% DMSO (100  $\mu$ L of media, per well). 24–72 h after treatment (as specified), medium was removed and cells were washed with 100  $\mu$ L of PBS and then fixed in 4% paraformaldehyde for 10 min at rt and stained with Hoechst nuclear stain at a final concentration of 10  $\mu$ g/mL in PBS for 10 min at rt. After fixing, the cells were stored in 100  $\mu$ L of PBS for imaging. Wells were imaged with an IN Cell 2000 automated cell imager at 10 $\times$  magnification with 9 images per well (complete coverage) in bright field and DAPI channel fluorescence, and images were analyzed for nuclei count by IN Cell developer software. EC<sub>50</sub> values were calculated in GraphPad Prism from normalized dose–response curves.

**Toxicity by CellTiter-Glo.** Cells were harvested, resuspended, and plated with a Wellmate liquid handler (Thermo Scientific) into 384-well plates and cultured for 24 h before dosing. Master compound plates were made with a Janus (PerkinElmer), then further diluted to achieve uniform final concentrations of DMSO of 0.1% in media for all treatment conditions. Compound treatments in media were added to the cell plates with a Matrix Platemate (Thermo Scientific). Cell viabilities were determined 72 h after treatment by Cell-Titer Glo assay (Promega) on the Envision multilabel plate reader (PerkinElmer). Relative luminescent units (RLU) were plotted against corresponding drug concentrations and fitted with a standard four-parameter sigmoidal curve with GraphPad Prism 6. Data were further fit for EC<sub>50</sub> shift parameters in GraphPad Prism 6 to determine EC<sub>50</sub>

ratios for 1/2. Data are reported as the EC<sub>50</sub> ratio, and error bars represent SEM ( $n = 3$ ). Data for cell lines in which EC<sub>50</sub> ratio fits were ambiguous,  $R^2$  values were less than 0.9, or response to the free drug was less than 40% were not reported.

**Quantitative PCR.** Cells were seeded at 300 000 cells per well in 6-well plates and grown to confluence and then collected with trypsin (0.05%), washed with PBS, and snap-frozen in liquid N<sub>2</sub> and then stored at  $-78$  °C. Cell pellets were processed for mRNA isolation using Qiagen RNeasy Mini Kit with QIAshredder lysate homogenizers and on column DNA digest. Isolated mRNA was analyzed for concentration and purity on a ThermoScientific NanoDrop 2000c spectrophotometer, and 1000 ng of mRNA from each sample was translated to cDNA using Invitrogen SuperScript III First-Strand Synthesis System. The resulting cDNA was used for qRT-PCR analysis (10 ng/reaction) with SsoAdvanced Universal SYBR Green Supermix in a Roche LightCycler 480. GAPDH was used as an endogenous control, and relative mRNA levels were calculated from a standard curve of pooled samples with LightCycler 480 software used for second derivative maximum analysis and standard curve fitting. Samples were prepared and run in biological triplicates, and error bars represent SEM. A list of the gene specific primers used is provided in the [Supporting Information](#).

**Maximum Tolerable Dose Studies.** To evaluate the tolerability of the experimental agents, groups of three NSG (NOD SCID gamma) mice were treated with three ip injections of test article (Q4d or Q7d in separate studies) in a formulation comprising 50:40:10 PEG 400/20% 2-hydroxypropylcyclodextrine in water/DMSO. Individual groups ( $n = 3$ ) received doses that increased in 2- or 3-fold steps until a given dose caused one or more mice in the group to reach protocol limits for tolerance ( $>20\%$  weight loss) at any point post dosing.

**Pharmacokinetics Studies.** To evaluate the in vivo pharmacokinetic properties of the experimental agents, female NSG mice were treated with a single ip injection of test compounds formulated in 50:40:10 PEG 400/20% 2-hydroxypropylcyclodextrine in water/DMSO. Blood samples were collected 5 min, 15 min, 30 min, 1 h, 2 h, 4 h, 8 h, 12 h, and 24 h after dosing (3 mice were sampled per time point; each group of mice was sampled  $\leq 3$  times over 24 h) and analyzed for plasma concentrations of each compound via MS/MS analysis conducted by Integrated Analytical Solutions, Inc. (Berkeley, CA). The resulting data were analyzed with WinNonlin software to calculate standard PK parameters.

**Efficacy Studies.** To evaluate the in vivo properties of the experimental agents, we used the heterotopic indirect tumor xenograft model in nude mice (NCR nu/nu, Taconic) and SCID-beige mice. Early passage PC-3 cells were harvested, and a cell suspension (1:1 serum free DMEM/Matrigel) was injected subcutaneously (sc) into the right flank of anesthetized donor nude mice ( $10^6$  cells/mouse in 0.1 mL). For MDA-MB-231 xenografts, cells were injected into the mammary fat pad of anesthetized female SCID-beige mice ( $10^6$  cells/mouse in 0.1 mL of PBS). When the mean tumor volume was  $250\text{--}400$  mm<sup>3</sup>, tumor-bearing mice were treated with the indicated doses of compounds formulated in 50:40:10 PEG 400/20% 2-hydroxypropylcyclodextrine in water/DMSO via ip administration with the indicated frequency. Tumor volume (by caliper) and mouse weight were monitored twice weekly.

## ■ ASSOCIATED CONTENT

### ■ Supporting Information

The Supporting Information is available free of charge on the [ACS Publications website](#) at DOI: [10.1021/acs.jmedchem.6b01470](https://doi.org/10.1021/acs.jmedchem.6b01470).

Supplemental tables, figures and schemes; synthetic procedures and compound characterization for new compounds; animal welfare statement; and a list of gene-specific primers used for qRT-PCR analysis ([PDF](#)) Molecular formula strings and some data ([CSV](#))

## ■ AUTHOR INFORMATION

### Corresponding Author

\*Phone: 415-514-9698. Fax: 415-514-4507. E-mail: [adam.renslo@ucsf.edu](mailto:adam.renslo@ucsf.edu).

### ORCID

Adam R. Renslo: [0000-0002-1240-2846](https://orcid.org/0000-0002-1240-2846)

### Present Address

<sup>†</sup>S.D.F.: Prolynx LLC, San Francisco, CA, 94158.

### Author Contributions

B.S., J.A.W., and A.R.R. designed compounds and conceived experiments. B.S. and S.D.F. synthesized compounds. B.S., S.D.F., Y.S., and B.H. acquired data. All authors analyzed the data. A.R.R. supervised the project. B.S. and A.R.R. wrote the manuscript. All authors reviewed, edited, and commented on the manuscript.

### Notes

The authors declare no competing financial interest.

## ■ ACKNOWLEDGMENTS

A.R.R. acknowledges funding from the U.S. National Institutes of Health (R01 Grant AI105106) and from the NIH National Center for Advancing Translational Science (UCSF-CTSI Grant UL1 TR000004). B.S. acknowledges funding from the NIH Research Training Grant in Chemistry and Chemical Biology (Grant T32 GM064337). The authors thank Prof. S. Bandyopadhyay (UCSF) for providing the MCF10A cell lines used in these studies, Steven Chen for technical support in automated cell imaging and image analysis with InCell Developer software, Dr. Tetsuya Matsuguchi for his assistance with qRT-PCR set up and analysis, Dr. Alan Wolfe for his assistance in calculating pharmacokinetic parameters, and the Preclinical Therapeutic Core at UCSF where in vivo experiments were performed.

## ■ ABBREVIATIONS USED

TAP, tumor-activated prodrug; ADC, antibody–drug conjugate; TRX, a 1,2,4-trioxolane scaffold for payload delivery; DXL, 1,3-dioxolane scaffold used as nonperoxidic controls; PURO, puromycin; qRT-PCR, quantitative real-time polymerase chain reaction; CBI, cyclopropylbenzindoline; MTD, maximally tolerated dose; Q4d, dosed every 4 days; Q7d, dosed every 7 days; ALT, alanine transaminase; AST, aspartate transaminase; CPK, creatine phosphokinase; H&E, hematoxylin and eosin stained; CL, clearance;  $F$ , fraction of drug achieving systemic exposure following an ip dose;  $V_z$ , volume of distribution; AUC, area under the curve

## ■ REFERENCES

- (1) Lorusso, P. M.; Edelman, M. J.; Bever, S. L.; Forman, K. M.; Pilat, M.; Quinn, M. F.; Li, J.; Heath, E. I.; Malburg, L. M.; Klein, P. J.; Leamon, C. P.; Messmann, R. A.; Sausville, E. A. Phase I study of folate conjugate EC145 (vintafolide) in patients with refractory solid tumors. *J. Clin. Oncol.* **2012**, *30*, 4011–4016.
- (2) Beck, A.; Reichert, J. M. Antibody-drug conjugates: present and future. *MAbs.* **2014**, *6*, 15–17.
- (3) Kratz, F.; Müller, I. A.; Rypa, C.; Warnecke, A. Prodrug strategies in anticancer chemotherapy. *ChemMedChem* **2008**, *3*, 20–53.
- (4) Brown, J. M.; Giaccia, A. J. The unique physiology of solid tumors: opportunities (and problems) for cancer therapy. *Cancer Res.* **1998**, *58*, 1408–1416.
- (5) Brown, J. M.; Wilson, W. R. Exploiting tumour hypoxia in cancer treatment. *Nat. Rev. Cancer* **2004**, *4*, 437–447.



- (6) Torti, S. V.; Torti, F. M. Iron and cancer: more ore to be mined. *Nat. Rev. Cancer* **2013**, *13*, 342–355.
- (7) Chaturvedi, D.; Goswami, A.; Saikia, P. P.; Barua, N. C.; Rao, P. G. Artemisinin and its derivatives: a novel class of anti-malarial and anti-cancer agents. *Chem. Soc. Rev.* **2010**, *39*, 435–454.
- (8) O'Neill, P. M.; Posner, G. H. A medicinal chemistry perspective on artemisinin and related endoperoxides. *J. Med. Chem.* **2004**, *47*, 2945–2964.
- (9) Mercer, A. E.; Copple, I. M.; Maggs, J. L.; O'Neill, P. M.; Park, B. K. The role of heme and the mitochondrion in the chemical and molecular mechanisms of mammalian cell death induced by the artemisinin antimalarials. *J. Biol. Chem.* **2011**, *286*, 987–996.
- (10) Mercer, A. E.; Maggs, J. L.; Sun, X.-M.; Cohen, G. M.; Chadwick, J.; O'Neill, P. M.; Park, B. K. Evidence for the involvement of carbon-centered radicals in the induction of apoptotic cell death by artemisinin compounds. *J. Biol. Chem.* **2007**, *282*, 9372–9382.
- (11) Dixon, S. J.; Stockwell, B. R. The role of iron and reactive oxygen species in cell death. *Nat. Chem. Biol.* **2014**, *10*, 9–17.
- (12) Pantopoulos, K. Iron metabolism and the IRE/IRP regulatory system: an update. *Ann. N. Y. Acad. Sci.* **2004**, *1012*, 1–13.
- (13) Wang, J.; Pantopoulos, K. Regulation of cellular iron metabolism. *Biochem. J.* **2011**, *434*, 365–381.
- (14) Richardson, D. R.; Ponka, P. The molecular mechanisms of the metabolism and transport of iron in normal and neoplastic cells. *Biochim. Biophys. Acta, Rev. Biomembr.* **1997**, *1331*, 1–40.
- (15) Boulton, J.; Roberts, K.; Brookes, M. J.; Hughes, S.; Bury, J. P.; Cross, S. S.; Anderson, G. J.; Sychal, R.; Iqbal, T.; Tselepis, C. Overexpression of cellular iron import proteins is associated with malignant progression of esophageal adenocarcinoma. *Clin. Cancer Res.* **2008**, *14*, 379–387.
- (16) Kakhlon, O.; Gruenbaum, Y.; Cabantchik, Z. Ferritin expression modulates cell cycle dynamics and cell responsiveness to H-ras-induced growth via expansion of the labile iron pool. *Biochem. J.* **2002**, *363*, 431–436.
- (17) Pinnix, Z. K.; Miller, L. D.; Wang, W.; D'Agostino, R.; Kute, T.; Willingham, M. C.; Hatcher, H.; Tesfay, L.; Sui, G.; Di, X.; Torti, S. V.; Torti, F. M. Ferroportin and iron regulation in breast cancer progression and prognosis. *Sci. Transl. Med.* **2010**, *2*, 43ra56.
- (18) Wu, K.-J.; Polack, A.; Dalla-Favera, R. Coordinated regulation of iron-controlling genes, H-ferritin and IRP2, by c-MYC. *Science* **1999**, *283*, 676–679.
- (19) Toyokuni, S. Role of iron in carcinogenesis: cancer as a ferrotoxic disease. *Cancer Sci.* **2009**, *100*, 9–16.
- (20) Miller, L. D.; Coffman, L. G.; Chou, J. W.; Black, M. A.; Bergh, J.; D'Agostino, R.; Torti, S. V.; Torti, F. M. An iron regulatory gene signature predicts outcome in breast cancer. *Cancer Res.* **2011**, *71*, 6728–6737.
- (21) Valecha, N.; Looareesuwan, S.; Martensson, A.; Abdulla, S. M.; Krudsood, S.; Tangpukdee, N.; Mohanty, S.; Mishra, S. K.; Tyagi, P. K.; Sharma, S. K.; Moehrle, J.; Gautam, A.; Roy, A.; Paliwal, J. K.; Kothari, M.; Saha, N.; Dash, A. P.; Björkman, A. Arterolane, a new synthetic trioxolane for treatment of uncomplicated *Plasmodium falciparum* malaria: a phase II, multicenter, randomized, dose-finding clinical trial. *Clin. Infect. Dis.* **2010**, *51*, 684–691.
- (22) Borstnik, K.; Paik, I.; Shapiro, T. A.; Posner, G. H. Antimalarial chemotherapeutic peroxides: artemisinin, yingzhaosu A and related compounds. *Int. J. Parasitol.* **2002**, *32*, 1661–1667.
- (23) Vennerstrom, J. L.; Arbe-Barnes, S.; Brun, R.; Charman, S. A.; Chiu, F. C.; Chollet, J.; Dong, Y.; Dorn, A.; Hunziker, D.; Matile, H.; McIntosh, K.; Padmanilayam, M.; Santo Tomas, J.; Scheurer, C.; Scoreaux, B.; Tang, Y.; Urwyler, H.; Wittlin, S.; Charman, W. N. Identification of an antimalarial synthetic trioxolane drug development candidate. *Nature* **2004**, *430*, 900–904.
- (24) Valecha, N.; Krudsood, S.; Tangpukdee, N.; Mohanty, S.; Sharma, S. K.; Tyagi, P. K.; Anvikar, A.; Mohanty, R.; Rao, B. S.; Jha, A. C.; Shahi, B.; Singh, J. P. N.; Roy, A.; Kaur, P.; Kothari, M.; Mehta, S.; Gautam, A.; Paliwal, J. K.; Arora, S.; Saha, N. Arterolane maleate plus piperazine phosphate for treatment of uncomplicated *Plasmodium falciparum* malaria: A comparative, multicenter, randomized clinical trial. *Clin. Infect. Dis.* **2012**, *55*, 663–671.
- (25) Creek, D. J.; Charman, W. N.; Chiu, F. C. K.; Prankerd, R. J.; Dong, Y.; Vennerstrom, J. L.; Charman, S. A. Relationship between antimalarial activity and heme alkylation for spiro- and dispiro-1,2,4-trioxolane antimalarials. *Antimicrob. Agents Chemother.* **2008**, *52*, 1291–1296.
- (26) Creek, D.; Charman, W.; Chiu, F. C. K.; Prankerd, R. J.; McCullough, K. J.; Dong, Y.; Vennerstrom, J. L.; Charman, S. A. Iron-mediated degradation kinetics of substituted dispiro-1, 2, 4-trioxolane antimalarials. *J. Pharm. Sci.* **2007**, *96*, 2945–56.
- (27) Tang, Y.; Dong, Y.; Wang, X.; Sriraghavan, K.; Wood, J. K.; Vennerstrom, J. L. Dispiro-1,2,4-trioxane analogues of a prototype dispiro-1,2,4-trioxolane: mechanistic comparators for artemisinin in the context of reaction pathways with iron(II). *J. Org. Chem.* **2005**, *70*, 5103–5110.
- (28) Wang, X.; Creek, D. J.; Schiaffo, C. E.; Dong, Y.; Chollet, J.; Scheurer, C.; Wittlin, S.; Charman, S. A.; Dussault, P. H.; Wood, J. K.; Vennerstrom, J. L. Spiroadamantyl 1,2,4-trioxolane, 1,2,4-trioxane, and 1,2,4-trioxepane pairs: relationship between peroxide bond iron(II) reactivity, heme alkylation efficiency, and antimalarial activity. *Bioorg. Med. Chem. Lett.* **2009**, *19*, 4542–4545.
- (29) Fontaine, S. D.; Dipasquale, A. G.; Renslo, A. R. Efficient and Stereocontrolled Synthesis of 1,2,4-trioxolanes useful for ferrous iron-dependent drug delivery. *Org. Lett.* **2014**, *16*, 5776–5779.
- (30) Fontaine, S. D.; Spangler, B.; Gut, J.; Lauterwasser, E. M. W.; Rosenthal, P. J.; Renslo, A. R. Drug delivery to the malaria parasite using an arterolane-like scaffold. *ChemMedChem* **2015**, *10*, 47–51.
- (31) Mahajan, S. S.; Deu, E.; Lauterwasser, E. M. W.; Leyva, M. J.; Ellman, J. A.; Bogyo, M.; Renslo, A. R. A fragmenting hybrid approach for targeted delivery of multiple therapeutic agents to the malaria parasite. *ChemMedChem* **2011**, *6*, 415–419.
- (32) Deu, E.; Chen, I. T.; Lauterwasser, E. M. W.; Valderramos, J.; Li, H.; Edgington, L. E.; Renslo, A. R.; Bogyo, M. Ferrous iron-dependent drug delivery enables controlled and selective release of therapeutic agents in vivo. *Proc. Natl. Acad. Sci. U. S. A.* **2013**, *110*, 18244–18249.
- (33) Lauterwasser, E. M. W.; Fontaine, S. D.; Li, H.; Gut, J.; Katneni, K.; Charman, S. A.; Rosenthal, P. J.; Bogyo, M.; Renslo, A. R. Trioxolane-mediated delivery of mefloquine limits brain exposure in a mouse model of malaria. *ACS Med. Chem. Lett.* **2015**, *6*, 1145–1149.
- (34) Spangler, B.; Morgan, C. W.; Fontaine, S. D.; Vander Wal, M. N.; Chang, C. J.; Wells, J. A.; Renslo, A. R. A reactivity-based probe of the intracellular labile ferrous iron pool. *Nat. Chem. Biol.* **2016**, *12*, 680–685.
- (35) Odlo, K.; Hentzen, J.; dit Chabert, J. F.; Ducki, S.; Gani, O. A. B. S. M.; Sylte, I.; Skrede, M.; Florenes, V. A.; Hansen, T. V. 1,5-Disubstituted 1,2,3-triazoles as cis-restricted analogues of combretastatin A-4: Synthesis, molecular modeling and evaluation as cytotoxic agents and inhibitors of tubulin. *Bioorg. Med. Chem.* **2008**, *16*, 4829–4838.
- (36) Martins, M. M.; Zhou, A. Y.; Corella, A.; Horiuchi, D.; Yau, C.; Rakshandehroo, T.; Gordan, J. D.; Levin, R. S.; Johnson, J.; Jascur, J.; Shales, M.; Sorrentino, A.; Cheah, J.; Clemons, P. A.; Shamji, A. F.; Schreiber, S. L.; Krogan, N. J.; Shokat, K. M.; McCormick, F.; Goga, A.; Bandyopadhyay, S. Linking tumor mutations to drug responses via a quantitative chemical-genetic interaction map. *Cancer Discovery* **2015**, *5*, 154–167.
- (37) Radulescu, S.; Brookes, M. J.; Salgueiro, P.; Ridgway, R. A.; McGhee, E.; Anderson, K.; Ford, S. J.; Stones, D. H.; Iqbal, T. H.; Tselepis, C.; Sansom, O. J. Luminal iron levels govern intestinal tumorigenesis after Apc loss in vivo. *Cell Rep.* **2012**, *2*, 270–282.
- (38) Yang, W. S.; Stockwell, B. R. Synthetic lethal screening identifies compounds activating iron-dependent, nonapoptotic cell death in oncogenic-RAS-harboring cancer cells. *Chem. Biol.* **2008**, *15*, 234–245.
- (39) Boger, D. L.; Johnson, D. S. CC-1065 and the duocarmycins: unraveling the keys to a new class of naturally derived DNA alkylating agents. *Proc. Natl. Acad. Sci. U. S. A.* **1995**, *92*, 3642–3649.

(40) Yang, S.; Denny, W. A. A new short synthesis of 3-substituted 5-amino-1-(chloromethyl)-1,2-dihydro-3H-benzo[e]indoles (amino-CBIs). *J. Org. Chem.* **2002**, *67*, 8958–8961.

(41) Atwell, G. J.; Milbank, J. J.; Wilson, W. R.; Hogg, A.; Denny, W. A. 5-Amino-1-(chloromethyl)-1,2-dihydro-3H-benz[e]indoles: relationships between structure and cytotoxicity for analogues bearing different DNA minor groove binding subunits. *J. Med. Chem.* **1999**, *42*, 3400–3411.

(42) Jeffrey, S. C.; Torgov, M. Y.; Andreyka, J. B.; Boddington, L.; Cervený, C. G.; Denny, W. A.; Gordon, K. A.; Gustin, D.; Haugen, J.; Kline, T.; Nguyen, M. T.; Senter, P. D. Design, synthesis, and in vitro evaluation of dipeptide-based antibody minor groove binder conjugates. *J. Med. Chem.* **2005**, *48*, 1344–1358.

(43) McGovren, J. P.; Clarke, G. L.; Pratt, E. A.; DeKoning, T. F. Preliminary toxicity studies with the DNA-binding antibiotic, CC-1065. *J. Antibiot.* **1984**, *37*, 63–70.

(44) Markovic, S. N.; Suman, V. J.; Vukov, A. M.; Fitch, T. R.; Hillman, D. W.; Adjei, A. A.; Alberts, S. R.; Kaur, J. S.; Braich, T. A.; Leitch, J. M.; Creagan, E. T. Phase II trial of KW2189 in patients with advanced malignant melanoma. *Am. J. Clin. Oncol.* **2002**, *25*, 308–312.

(45) Workman, P. Genomics and the second golden era of cancer drug development. *Mol. Biosyst.* **2005**, *1*, 17–26.

(46) Lord, C. J.; Ashworth, A. The DNA damage response and cancer therapy. *Nature* **2012**, *481*, 287–294.

(47) Taylor, C. W.; Kim, Y. S.; Childress-Fields, K. E.; Yeoman, L. C. Sensitivity of nuclear c-Myc levels and induction to differentiation-inducing agents in human colon tumor cell lines. *Cancer Lett.* **1992**, *62*, 95–105.

(48) Horiuchi, D.; Anderton, B.; Goga, A. Taking on Challenging Targets: Making Myc druggable. *Am. Soc. Clin. Oncol. Educ. B* **2014**, *34*, e497–502.